Molecular Therapy
Original Article

RNA base editing therapy cures hearing loss induced by *OTOF* gene mutation

Yuanyuan Xue,[1,2,9] Yong Tao,[1,4,5,9] Xing Wang,[2,9] Xueling Wang,[1,4,5] Yilai Shu,[6,7,8] Yuanhua Liu,[3] Wen Kang,[1,4,5] Sifan Chen,[2] Zhenzhe Cheng,[1,4,5] Boou Yan,[2] Yanwei Xie,[2] Lanting Bi,[2] Haitao Jia,[2] Jinhui Li,[2] Qingquan Xiao,[2] Liying Chen,[2] Xuan Yao,[2] Linyu Shi,[2] Hui Yang,[2,3] and Hao Wu[1,4,5]

[1]Department of Otolaryngology-Head and Neck Surgery, Shanghai Ninth People's Hospital, Shanghai Jiaotong University School of Medicine, Shanghai 200011, China; [2]HuidaGene Therapeutics Co., Ltd., Shanghai 200131, China; [3]Institute of Neuroscience, Center for Excellence in Brain Science and Intelligence Technology, Chinese Academy of Sciences, Shanghai 200031, China; [4]Ear Institute, Shanghai Jiaotong University School of Medicine, Shanghai 200125, China; [5]Shanghai Key Laboratory of Translational Medicine on Ear and Nose Diseases, Shanghai 200125, China; [6]ENT Institute and Department of Otorhinolaryngology, Eye and ENT Hospital, State Key Laboratory of Medical Neurobiology and MOE Frontiers Center for Brain Science, Fudan University, Shanghai 200031, China; [7]Institute of Biomedical Science, Fudan University, Shanghai 200032, China; [8]NHC Key Laboratory of Hearing Medicine, Fudan University, Shanghai 200032, China

Otoferlin (OTOF) gene mutations represent the primary cause of hearing impairment and deafness in auditory neuropathy. The c.2485C>T (p. Q829X) mutation variant is responsible for approximately 3% of recessive prelingual deafness cases within the Spanish population. Previous studies have used two recombinant AAV vectors to overexpress OTOF, albeit with limited efficacy. In this study, we introduce an enhanced mini-dCas13X RNA base editor (emxABE) delivered via an AAV9 variant, achieving nearly 100% transfection efficiency in inner hair cells. This approach is aimed at treating *OTOF*^{Q829X}, resulting in an approximately 80% adenosine-to-inosine conversion efficiency in humanized *Otof*$^{Q829X/Q829X}$ mice. Following a single scala media injection of emxABE targeting *OTOF*^{Q829X} (emxABE-T) administered during the postnatal day 0–3 period in *Otof*$^{Q829X/Q829X}$ mice, we observed OTOF expression restoration in nearly 100% of inner hair cells. Moreover, auditory function was significantly improved, reaching similar levels as in wild-type mice. This enhancement persisted for at least 7 months. We also investigated P5–P7 and P30 *Otof*$^{Q829X/Q829X}$ mice, achieving auditory function restoration through round window injection of emxABE-T. These findings not only highlight an effective therapeutic strategy for potentially addressing *OTOF*^{Q829X}-induced hearing loss but also underscore emxABE as a versatile toolkit for treating other monogenic diseases characterized by premature termination codons.

INTRODUCTION

Hearing loss represents a widespread sensory disorder, affecting approximately 466 million individuals globally, which accounts for roughly 5% of the world's population.[1] This condition imposes a substantial burden on society and significantly contributes to global disability.[2] In developed countries, congenital hearing loss affects approximately 1 in 500 newborns, with over half of these cases attributed to genetic factors,[1,3] which can be categorized as either dominant or recessive hearing loss.

Mutations within the *OTOF* gene, responsible for encoding otoferlin, are associated with prelingual and profound recessive hearing loss, as evidenced by abnormal or absent auditory brainstem responses (ABRs) and preserve otoacoustic emissions (OAEs) or cochlear microphonics in newborn hearing screening.[4] Otoferlin is prominently expressed in the sensory inner hair cells (IHCs) of the cochlea, playing a crucial role in synaptic transmission from the auditory sensory cells, the IHCs, to the spiral ganglion neurons (SGNs) of the auditory nerve.[5,6] Consequently, *OTOF* mutations are classified as auditory neuropathy (AN), also known as DFNB9,[4] an autosomal recessive AN. The c.2485C>T (p. Q829X) nonsense mutation in the *OTOF* gene, located on exon 22 of chromosomal region 2p22-23, is responsible for approximately 3% of all of the cases of recessive prelingual deafness, primarily observed in the Spanish population, followed by the Mexican, English, French, and Argentine populations.[7]

Notably, the hearing loss stemming from *OTOF* gene mutations represents a significant unmet medical need, particularly in light of the absence of curative therapies for individuals with genetic hearing impairment. Presently, the primary available treatment for patients with *OTOF* mutations and profound hearing loss is cochlear implantation (CI), a device that circumvents the affected IHC synapses by directly stimulating the SGNs electrically. Nevertheless, CI recipients often encounter difficulties in speech perception within noisy environments[8] or when appreciating music.[9] Moreover, individuals receiving CI at a young age may require subsequent surgeries to adjust

Received 20 July 2023; accepted 30 October 2023;
https://doi.org/10.1016/j.ymthe.2023.10.019.

[9]These authors contributed equally

Correspondence: Hui Yang, HuidaGene Therapeutics Co., Ltd., Shanghai 200131, China.
E-mail: huiyang@huidagene.com
Correspondence: Hao Wu, Department of Otolaryngology-Head and Neck Surgery, Shanghai Ninth People's Hospital, Shanghai Jiaotong University School of Medicine, Shanghai 200011, China.
E-mail: wuhao@shsmu.edu.cn

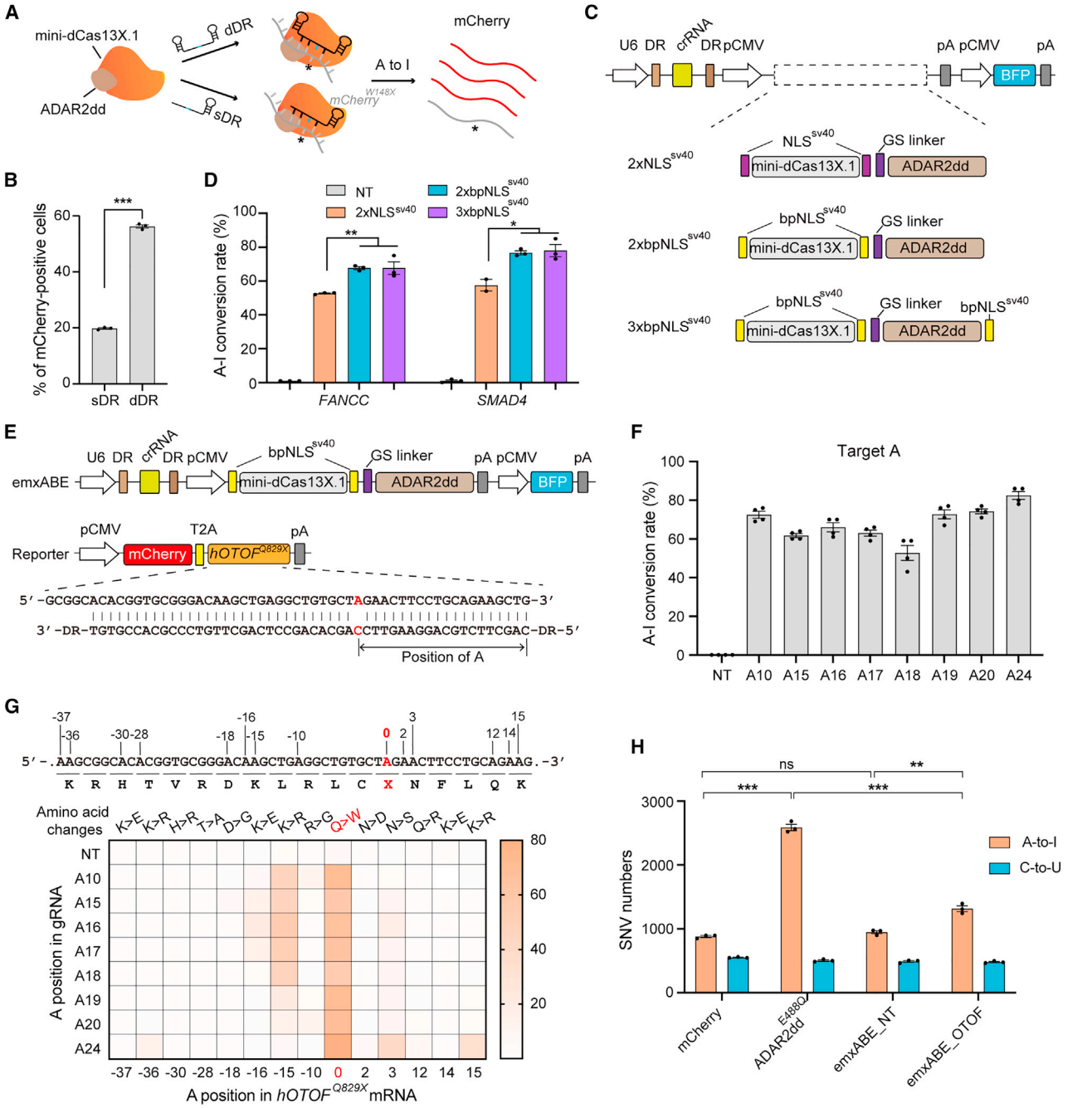

Figure 1. Screen of efficient RNA base editor and gRNAs for efficiently correcting *hOTOF*^{Q829X} mutation

(A) Schematic illustration of RNA base editing mediated by single direct repeat (sDR) or dual direct repeat (dDR) elements. The RNA base editor consists of mini-dCas13X.1 protein and ADAR2dd protein from the RESCUE-S editor.[18] The reporter contains a mCherry CDS with a stop codon at W148 (TGG>TAG). Red fluorescence (mCherry) can only be detected if A-to-I conversion is achieved. (B) Flow cytometry results of editors with different gRNA components. The higher the mCherry ratio, the higher the efficiency of A-to-I conversion. (C) Schematic illustration of RNA base editors with different subcellular localization sequences. NLS^{SV40}, NLS from simian virus 40; bpNLS^{SV40}, bipartite SV40 NLS. (D) A-to-I conversion rate of RNA base editors with different subcellular localization sequences at two endogenous sites in HEK293T cells. n = 3, except for 2xNLS^{SV40} at *SMAD4* site, where n = 2. (E) Schematic diagram of screening optimal gRNAs targeting *hOTOF*^{Q829X} mutation in HEK293T cells. The reporter construct contains an mCherry cassette fused with 2A peptide and part of *hOTOF* CDS with Q829X (CAG>TAG) mutation. The red C indicates mismatched base against A mutation in *hOTOF* transcript. pCMV, porcine cytomegalovirus. (F) A-to-I conversion efficiency of gRNAs containing different mismatch base positions. NT, nontargeting crRNA. n = 4. (G) Measurement of bystander A-to-I editing rate for multiple adenosines within targeting sequence of all gRNAs from deep sequencing. The targeting site number is 0. Others

(legend continued on next page)

for implant displacement as the skull undergoes growth and changes in shape.[10] Moreover, complication of CI occurred in an estimated 5%–10% cases including intrinsic device failure and non-device related failure such as cochlear implant extrusion (CIE).[11] Given the limited effectiveness of the current intervention, which fails to restore "normal" hearing, the development of innovative therapeutic approaches capable of delivering a precise, one-time, enduring cure for the restoration or prevention of genetic hearing loss is of paramount importance.

Recent studies have explored a dual-adeno-associated virus (AAV) gene therapy approach for the treatment of *OTOF* gene mutations.[12–14] However, the restricted cargo capacity of AAV poses a significant challenge when delivering the approximately 6-kb otoferlin gene. In these investigations, the *OTOF* cDNA was divided into two AAV vectors, each containing a portion of the extensive transgene expression cassette, circumventing the limitations of AAV packaging capacity (approximately 4.7 kb). This approach resulted in otoferlin expression levels of 50%–70% in IHCs and only partial restoration of auditory function.

Previously, we reported the use of a smaller size and lower off-target RNA editing tool, mxABE,[15] to achieve adenosine-to-inosine (A-to-I) conversion and partially restored autosomal dominant hearing loss through *in vivo* AAV delivery. However, we observed that the editing efficiency in homozygous mice was 4.22% ± 0.68%,[16] highlighting the need for improving the editing efficiency. To enhance therapeutic outcomes, we have further refined and optimized the mxABE tool, with a focus on minimizing off-target effects. In addition, we engineered an AAV9 variant in-house, demonstrating an exceptional transfection efficiency of nearly 100% in IHCs (referred to as AAV-HGHC; Table S15). Subsequently, we investigated an enhanced mini-dCas13X RNA base editor (emxABE), delivered using AAV-HGHC for the treatment of the $OTOF^{Q829X}$ (CAG>TAG) mutation in the humanized *Otof* $^{Q829X/Q829X}$ mouse model, facilitating the conversion of TAG to TGG at the RNA level. Our innovative strategy achieved an approximate 80% A-to-I (TAG>TGG) conversion efficiency, resulting in nearly 100% otoferlin expression in the IHCs and the restoration of auditory function to wild-type (WT) levels, sustaining these improvements for at least 7 months.

RESULTS

Optimization of an efficient mini-dCas13X RNA base editor, emxABE

In our previous study, we reported that the mini-dCas13X-mediated RNA base editor mxABE[16] exhibited the potential to partially restore auditory function in individuals with autosomal dominant inherited hearing loss. However, the *in vivo* editing efficiency proved insufficient.[16] Therefore, we undertook efforts to enhance the base editing efficiency within the mxABE system. Previous research indicated that double-direct repeats (DRs) resulted in higher base editing efficiency than single DRs in the MS2-based RNA base editing system.[17] Thus, we investigated whether a double-DR strategy could similarly enhance mini-dCas13X-based RNA base editing. Initially, we observed that the mini-dCas13X.1 protein lost its DR processing capability in comparison to the full-length dCas13X.1 protein when a DR sequence was inserted between the ATG and EGFP transcripts (Figures S1A and S1B). Subsequently, we cotransfected mxABE, an mCherry reporter system incorporating a stop codon at the W148 site, along with single-DR or double-DR guide RNA (gRNA) targeting the stop codon into human embryonic kidney (HEK) 293T cells. We quantified mCherry$^+$ cells 48 h later (Figure 1A). Flow cytometry analysis revealed that mxABE with the double-DR element demonstrated higher efficiency compared to mxABE with single DR (Figure 1B).

In addition, we optimized the nuclear localization signal (NLS) of mxABE, a modification previously suggested to enhance the efficiency of DNA base editors[19] (Figure 1C). Sanger sequencing results demonstrated that mxABE with $2xbpNLS^{SV40}$ or $3xbpNLS^{SV40}$ exhibited greater efficiency than mxABE with $2xNLS^{SV40}$ (Figure 1D). Subsequently, we referred to the more efficient mxABE, featuring both the double-DR and $2xbpNLS^{SV40}$ modifications, as enhanced mxABE (emxABE). We then compared the editing efficiency at the $Myo6^{C442Y}$ site[16] between mxABE and the optimized emxABE editor, revealing that emxABE exhibited higher base editing efficiency than mxABE (Figures S1C and S1D). As a result, emxABE was selected for further experiments.

Screen of gRNAs for $OTOF^{Q829X}$ correction

To establish an *in vitro* readout of $OTOF^{Q829X}$ correction efficiency, we fused mutant $OTOF^{Q829X}$ with mCherry using a T2A sequence to overexpress $OTOF^{Q829X}$ RNA. We cotransfected this construct with the plasmid containing emxABE, blue fluorescent protein (BFP), and various gRNAs targeting the Q829X mutation in HEK293T cells (Figure 1E; Table S1). The base editing activity was assessed by Sanger sequencing of mCherry-$OTOF^{Q829X}$ fusion RNA in BFP$^+$/mCherry$^+$ cells. The gRNAs carrying mismatched nucleotides against the Q829X mutation at different positions exhibited slightly variable efficiency, ranging from 52.75% ± 7.76% to 82.50% ± 4.12% (Figure 1F). In addition to targeted editing, different gRNAs displayed varying degrees of bystander editing at multiple sites, as revealed by deep sequencing analysis (Figure 1G). We selected the gRNA targeting the Q829X mutation with a mismatch at position A19, because it demonstrated high targeted editing and minimal bystander editing, for the subsequent experiments.

are sites with bystander editing, with -on the left and + on the right, which was omitted. Numbers represent the distance from the targeting site. The lower row is the corresponding amino acid, where X represents a stop codon. The top of the heatmap is the amino acid changes caused by bystander editing. The left side of > is the original amino acid; the right side of > is the amino acid after bystander editing. n = 1. (H) Transcriptome-wide off-target site numbers for mCherry (control), $ADAR2dd^{E488Q}$, emxABE_NT, or emxABE_OTOF, cotransfected with the $OTOF^{Q829X}$ reporter plasmid, in HEK293T cells. All of the values are presented as mean ± SEM, n = 3, unless otherwise noted. *$p < 0.05$, **$p < 0.01$, and ***$p < 0.001$, 2-tailed unpaired 2-sample t test. See Table S3 for detailed data.

To investigate potential off-target effects of *OTOF*^{Q829X}-targeting emxABE, we conducted transcriptome-wide RNA sequencing (RNA-seq) analysis on cells transfected with emxABE_OTOF (emxABE with gRNA targeting *OTOF*^{Q829X}), emxABE_NT (emxABE with a nontargeted gRNA), ADAR2dd^{E488Q}, and mCherry, all cotransfected with the *OTOF*^{Q829X} reporter in HEK293T cells (Figure S2A). In line with previously reported results,[16] cells treated with ADAR2dd^{E488Q} displayed higher levels of off-target edits than control cells treated solely with mCherry. The introduction of OTOF gRNA (emxABE_OTOF) resulted in a slightly higher number of (SNVs, albeit significantly fewer than cells treated with ADAR2dd^{E488Q} alone (Figures 1H and S2B). Further analysis revealed that emxABE and gRNA-induced SNVs led to only minimal amino acid changes in affected genes, primarily affecting biological regulation, cellular processes, and metabolic processes, with no notable impact on apoptosis pathways. This outcome may be attributed to the cellular stress regulation resulting from cell transfection (Figure S3).

Considering its high editing efficiency, minimal off-target edits, and relatively compact size (830 amino acids in total), we selected emxABE with the gRNA targeting the Q829X mutation, with a mismatch at position A19 for subsequent *in vivo* experiments using the *Otof* $^{Q829X/Q829X}$ mouse model.

In vivo RNA base editing with emxABE-T restored the otoferlin protein expression in P0–P3 humanized *Otof* $^{Q829X/Q829X}$ mice

To validate the *in vivo* editing efficiency, we established a humanized *Otof* $^{Q829X/Q829X}$ mouse model. Mouse *Otof* exon 21 was deleted using CRISPR-Cas9 guided by four single guide RNAs (sgRNAs) flanking exon 21 and replaced with the corresponding human exon containing the Q829X mutation (Figure S4A). These humanized *Otof* $^{Q829X/Q829X}$ mice exhibited profound deafness, with no detectable ABRs in response to tone-burst sound stimuli at 4 and 30 weeks (Figures S4B and S4C). However, distortion product OAEs (DPOAEs), assessing outer hair cell (OHC) amplification, remained nearly normal in these mice at 4 and 30 weeks (Figures S4B and S4C). This observation indicated that the impairment was specifically attributed to a defect in the IHCs, consistent with previous findings in *Otof* knockout mouse models.[12,13] In comparison with *Otof* $^{+/+}$ (WT) and *Otof* $^{+/Q829X}$ (Het) mice, *Otof* $^{Q829X/Q829X}$ (Homo) mutants did not express otoferlin protein (Figures S4D and S4E). Furthermore, the *Otof*$^{Q829X/Q829X}$ mutation did not affect the survival of hair cells (IHCs and OHCs) at 4 (Figures S4D and S4F) or 30 weeks (Figures S4E and S4F), providing a window of opportunity for molecular therapeutic experiments.

To confirm the *in vivo* activity of emxABE against the Q829X mutation, we delivered emxABE and gRNA targeting the Q829X mutation with a mismatch at A19 (hereafter referred to as emxABE-T) into AAV-HGHC (Figure 2A), an in-house-developed AAV9 variant with high transduction efficiency (>90%) in IHCs on postnatal day (P) 0–P3, P5–P7, and P30 mice (Figure S5). We injected AAV-HGHC–mediated emxABE-T unilaterally into the right inner ear of *Otof*$^{Q829X/Q829X}$ mice at P0–P3 via the scala media (SM). Four weeks postinjection, we dissected the inner ear soft tissue from the injected cochlea to analyze the adenine-to-guanine (A-to-G) editing efficiency of emxABE-T. Targeted deep sequencing results revealed a dose-dependent increase in A-to-G editing efficiency, ranging from 45.25% ± 6.14% at a low dose to 74.78% ± 3.04% at a medium dose (Figure 2B), indicating efficient correction of the stop codon (*Otof*^{Q829X}) to a readthrough (*Otof*^{Q829W}) allele through RNA base editing. Notably, we observed no increase in SNVs in the emxABE-T-treated mice compared to the vehicle-injected mice, as demonstrated by transcriptome-wide RNA-seq analysis, suggesting the high *in vivo* specificity of emxABE-T treatment (Figure S7E).

AAV-mediated otoferlin expression is primarily restricted to sensory IHCs in the cochlea.[12,13] Following a 4-week injection of medium-dose emxABE-T into *Otof*$^{Q829X/Q829X}$ mice, otoferlin protein was re-expressed throughout the cochlea, with 100% expression in virus-infected IHCs (Figures 2C and S6). This expression persisted for 30 weeks after injection (Figures 2D, 2E, and S6E). In contrast, no OTOF^{+} cells were observed in the cochlea injected with the vehicle. Previous studies indicated that *Otof* $^{-/-}$ mice have normal numbers of ribbon synapses at P6, with only 60% of these synapses persisting after P15.[20] Therefore, we investigated whether emxABE-T treatment in mice at P0–P3 could halt the decline in ribbon synapses. After 4 weeks of injection, the number of synaptic ribbons in the cochlea treated with emxABE-T was higher than in the vehicle-injected cochlea, with the basal turn being comparable to that of the WT cochlea. This finding indicated that emxABE-T treatment could prevent the loss of synapses in *Otof* $^{Q829X/Q829X}$ mice (Figures S6A–S6D). The recovery of CTBP2-labeled synaptic ribbon numbers was maintained for at least 30 weeks after injection (Figures 2D and 2F).

AAV-mediated emxABE-T restored hearing function in P0–P3 humanized *Otof* $^{Q829X/Q829X}$ mice

To evaluate the therapeutic effect of emxABE-T on hearing function in *Otof*$^{Q829X/Q829X}$ mice, we examined the ABRs to broadband clicks and tone bursts (Figure 2A). After 4 weeks of injection, ABR waves I–V were clearly identifiable in the emxABE-T group, similar to WT mice, whereas no identifiable ABR waveforms were elicited in the vehicle-treated *Otof* $^{Q829X/Q829X}$ mice (Figure 3A).

To assess the sensitivity of ears to specific frequencies, we analyzed the tone-burst ABR thresholds of treated *Otof* $^{Q829X/Q829X}$ mice. After 4 weeks of treatment, the ABR thresholds of ears treated with different doses of emxABE-T were restored to near-WT levels at every frequency (Figure 3B). This restoration was sustained for at least 30 weeks (Figures 3E, S7C, and S7D). In contrast, all of the *Otof*$^{Q829X/Q829X}$ mice treated with the vehicle showed no improvement in ABRs (Figures 3B and 3E, S7C, and S7D), confirming that the phenotypic improvement resulted from the specific correction of *Otof*^{Q829X} RNA. When stimulated by a 90-dB sound, the ABR wave I latency of the emxABE-T-treated ears was similar to that of the WT ears at 8, 16, and 32 kHz (Figure 3C). In addition, the ABR wave I amplitude, representing the summed electrical responses of primary auditory neurons to sound stimuli, increased to WT levels only at 8 kHz but not at 16 or 32

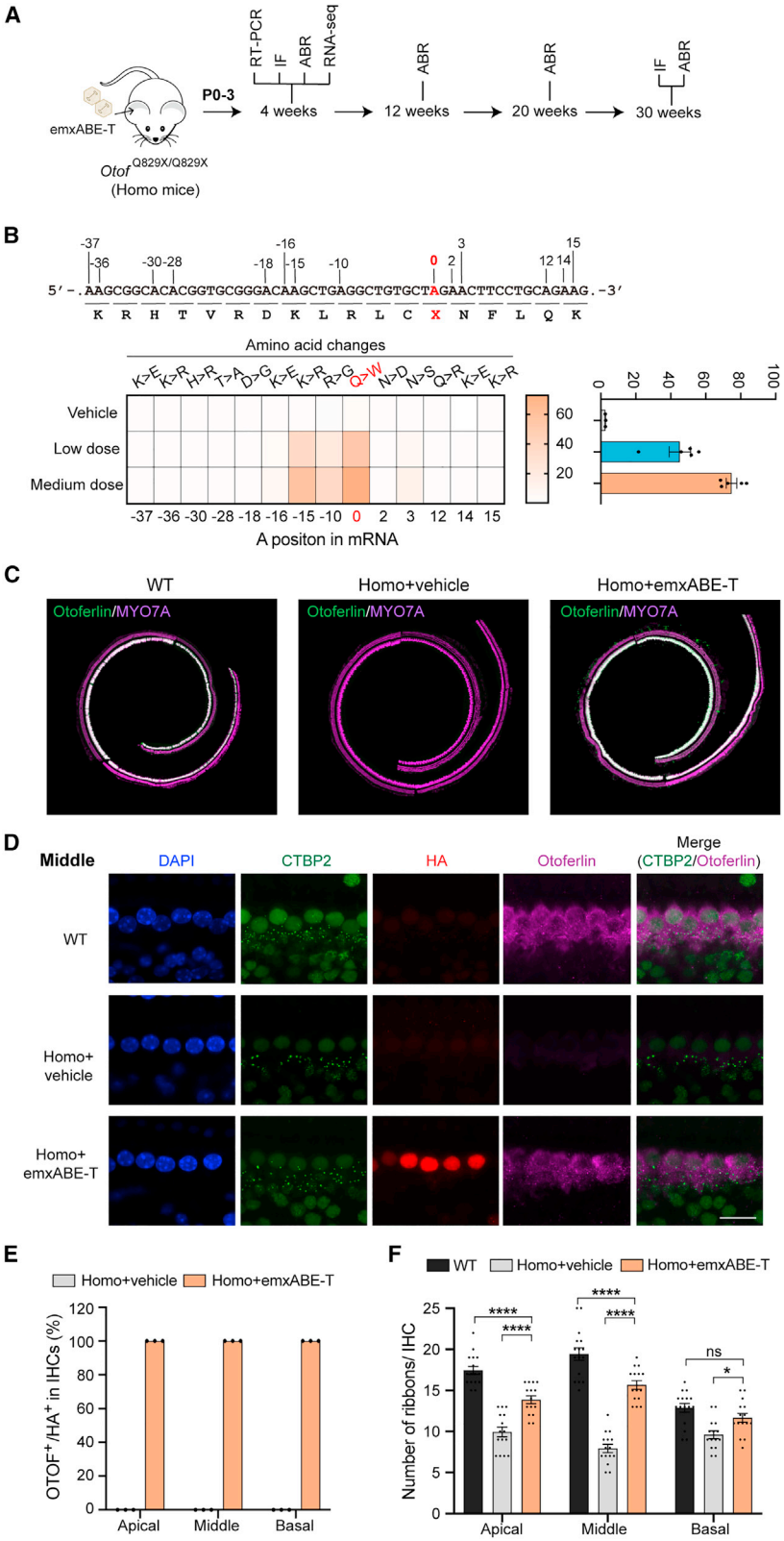

Figure 2. *In vivo* correction of *Otof* ^{Q829X} mutation and restoration of OTOF protein expression with emxABE-T delivered by AAV-HGHC at P0–P3 *Otof* $^{Q829X/Q829X}$ mice

(A) Diagrammatic workflow of the *in vivo* studies with emxABE-T by AAV-HGHC via SM injection at P0–P3 *Otof* $^{Q829X/Q829X}$ mice (hereafter marked Homo). IF, immunofluorescence staining. (B) Deep-sequencing results in the cochlea of *Otof* $^{Q829X/Q829X}$ mice injected with vehicle or low and medium doses of emxABE-T after 4 weeks of administration (vehicle, n = 3; low dose, n = 5; medium dose, n = 5). Targeting site number. Others are sites with bystander editing, with -on the left and + on the right. Numbers represent the distance from the targeting site. The lower row is the corresponding amino acid, and X represents a stop codon. The top of the heatmap is the amino acid changes caused by bystander editing. The left side of > is the original amino acid, the right side of > is the amino acid after bystander editing. On the right is the statistical analysis of editing efficiency at the only on-target site. (C) The confocal immunofluorescence results of the entire basilar membrane of mice after 4 weeks of virus injection. MYO7A$^+$ indicates the HC marker. n = 1. (D) High-magnification views of IHCs immunolabeled for synaptic ribbons (CTBP2) of middle cochlear turns after 30 weeks of virus injection. n = 3. Scale bar: 15 μm. HA tag indicates the expression of emxABE. (E) The proportion of successful recovery of OTOF protein expression in IHC cells infected with the virus (HA$^+$). n = 3. (F) Synaptic ribbon numbers quantified from IHCs in apical, middle, and basal cochlear turns after 30 weeks of administration (WT, n = 16 IHCs; Homo+vehicle, n = 15 IHCs; Homo+emxABE-T, n = 15 IHCs from 3 mice). HC, hair cell. Data are presented as mean ± SEM. Statistical tests are 2-way ANOVA with Bonferroni correction for multiple comparisons. *p < 0.05; ****p < 0.0001; ns, not statistically significant. Unless otherwise specified, Homo+ emxABE-T indicates the result of medium dose administration. See Table S4 for detailed data.

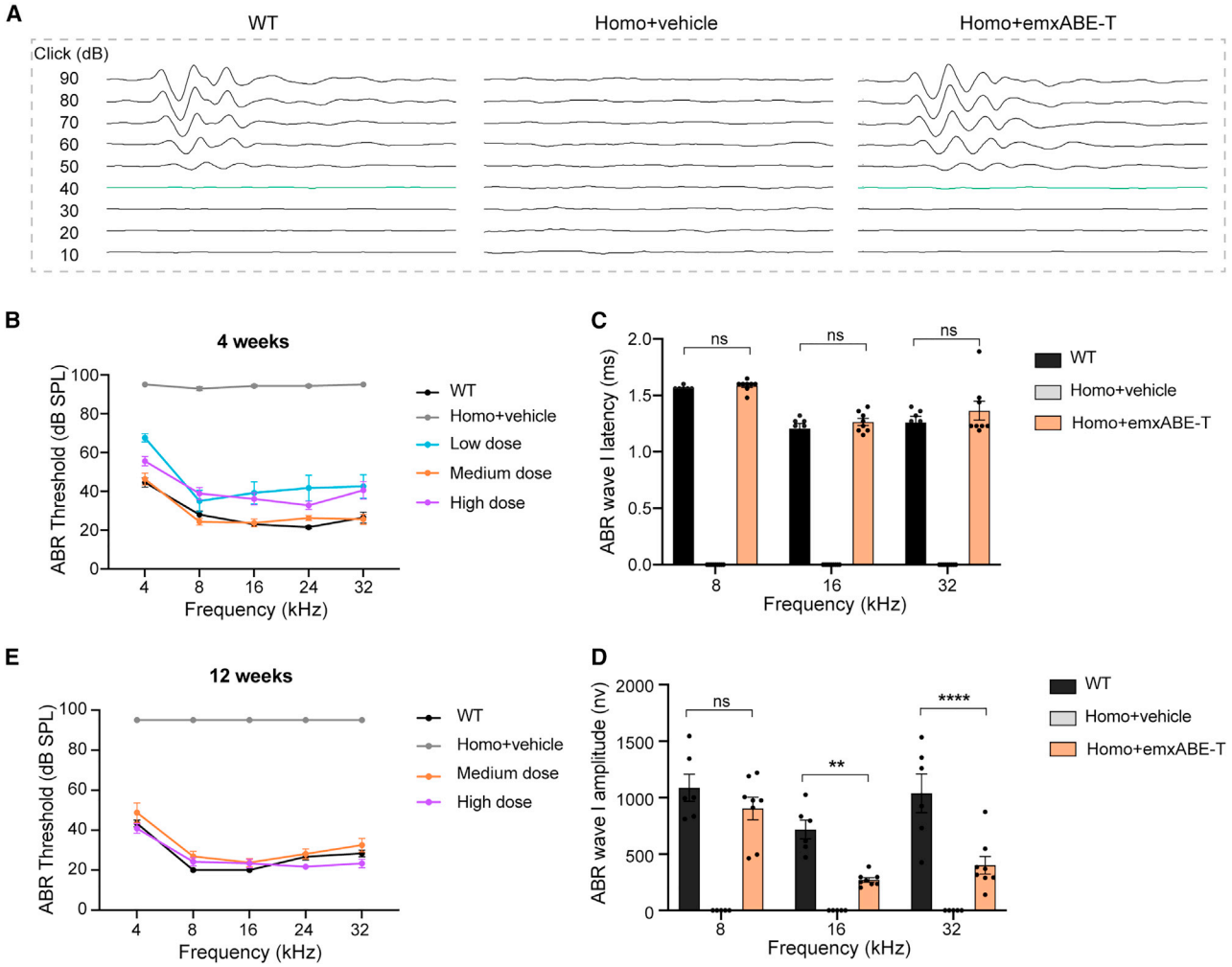

Figure 3. Recovery of hearing function of *Otof* ^{Q829X} with AAV-emxABE-T injection at P0–P3

(A) A representative graph of the Click ABR waveform recorded after 4 weeks of ear administration. The green trace represents the threshold of the mouse ears, with no threshold for the group of Homo+vehicle. (B) ABR thresholds of mice for tone-burst stimuli are recorded 4 weeks after therapeutic injection of low, medium, and high doses (WT, n = 10; Homo+vehicle, n = 7; low dose, n = 6; medium dose, n = 8; high dose, n = 9). (C and D) ABR wave I latency (C) and amplitude (D) at 8,16, and 32 kHz after 4 weeks of administration. (Latency: WT, n = 7; Homo+vehicle, n = 9; Homo+emxABE-T, n = 8. Amplitude: WT, n = 6; Homo+vehicle, n = 5; Homo+emxABE-T, n = 8.) (E) ABR thresholds of mice for tone-burst stimuli are recorded 12 weeks after therapeutic injection under medium and high dose (WT, n = 3; Homo+vehicle, n = 5; medium dose, n = 8; high dose, n = 6). Data are presented as mean ± SEM. Statistical tests were 2-way ANOVA with Bonferroni correction for multiple comparisons. **p < 0.01; ****p < 0.0001. Homo, *Otof* $^{Q829X/Q829X}$ mice. Unless otherwise specified, Homo+emxABE-T indicates the result of medium-dose administration. See Table S5 for detailed data.

kHz testing frequencies (Figure 3D). Injection with a high dose of emxABE-T restored both the latency and amplitude to WT levels at all of the testing frequencies (Figures S7A and S7B), further supporting the dose-dependent rescue of hearing ability.

In vivo editing and functional rescue in P5–P7/P30 humanized *Otof* $^{Q829X/Q829X}$ mice and P30 *Otof* $^{-/Q829X}$ mice

Considering that the human inner ear is fully developed *in utero* and the cochlea in P0–P3 mice is temporally equivalent to the human cochlea before 26 weeks' gestational age, we assessed the auditory function of *Otof* $^{Q829X/Q829X}$ mice after injecting emxABE-T via the round window (RW) on P5–P7 or P30 mice (Figures 4A and S8A), which corresponded to the late stages of human embryo development or postbirth.[12,21,22] After 3 or 4 weeks of injection, we observed an increase in A-to-G editing efficiency of up to 80% (P5–P7 injection) or 40% (P30 injection) (Figures 4B and S8B), respectively. Furthermore, the ratio of otoferlin expression restoration was nearly 100% in both P5–P7 and P30 treated mice, similar to that in P0–P3 treated mice (Figures 4D, 4E, S9, and S10).

Subsequently, we evaluated auditory function. After 3 weeks of injection, the hearing in the treated ears of P5–P7 *Otof* $^{Q829X/Q829X}$ mice

was rescued to nearly WT levels at different frequencies, and this improvement persisted for at least 19 weeks. Moreover, the latency and amplitude also returned to WT levels (Figures S8C–S8F). In addition, the hearing function of the treated P30 *Otof* $^{Q829X/Q829X}$ mice showed significant improvement, although differences remained compared to untreated WT mice (Figure 4F). This outcome could be attributed to injection-related injury or the relatively lower infection efficiency of emxABE-T in the cochlea of P30 mice (Figure 4F). Nonetheless, these results collectively demonstrate the effective rescue of auditory function by emxABE-T.

Given that a substantial proportion of patients with the Q829X mutation carry compound heterozygous mutations, where one allele is Q829X and the other is a mutation causing loss of function, we also established a mouse model of *Otof* $^{-/Q829X}$. Injecting emxABE-T into the cochlea of P30 mice significantly improved the hearing function of treated P30 *Otof* $^{-/Q829X}$ mice, although differences remained compared to untreated WT mice after 3 weeks (Figure S11). In summary, these findings indicate that emxABE-T exhibits promising therapeutic effects on both homozygous and heterozygous mice with Q829X mutations, further supporting the potential for clinical translation.

DISCUSSION

The inner ear, being a fluid-filled sensory organ, offers an ideal environment for the widespread diffusion of the delivered genes, making gene therapy an attractive strategy for addressing inner ear dysfunction.[1,3] Multiple preclinical studies have successfully used AAV-mediated gene replacement, delivering functional cDNA into the inner ear to correct genetic defects in mouse models of human recessive deafness.[23–27] However, these gene replacement approaches have limitations, including a narrow window of effectiveness and uncontrolled gene expression.[28] In this study, we introduced an enhanced RNA base editor (emxABE) delivered by AAV-HGHC, which exhibits high transduction efficiency in IHCs for the treatment of *Otof*$^{Q829X/Q829X}$ mice. Through the conversion of TAG mutations to TGG at the RNA level, we achieved the restoration of otoferlin expression in nearly 100% of IHCs and the restoration of the auditory function to WT levels for at least 7 months in *Otof*$^{Q829X/Q829X}$ mice.

For the first time, we have demonstrated an increase in synapses of IHCs (Figures 2F and S6) and a complete recovery of latency and wave I amplitude in emxABE-T-treated mice (Figures S7 and S8). This result highlights the potential of our RNA base editing strategy, characterized by improved AAV transduction rates and higher editing efficiency, for the treatment of inherited hearing loss.

Concerns regarding off-target activities of genome targeting platforms are significant in gene editing therapeutic applications.[29] Although we observed a slight increase in SNVs in cultured cells treated with emxABE-T, possibly due to the high copy number of emxABE-T in transfected cells, we found no increase in SNVs in the treated cochlea *in vivo*. This suggests the high specificity of emxABE-T in the treatment of *Otof*$^{Q829X/Q829X}$ mice. Furthermore, the bystander edits within editing windows could be minimized by introducing bulges at all bystander-edited adenosines.[30] Importantly, in this study, we did not observe any trend of hearing loss in treated mice for at least 30 weeks.

In conclusion, our data provide compelling proof-of-concept evidence that a single AAV vector combined with the RNA base editor approach is effective in restoring auditory function, with the potential for reduced manufacturing costs using a single AAV vector. Our cutting-edge therapeutic strategy holds promise for the potential of RNA base editing therapy to cure patients with inherited deafness.

MATERIALS AND METHODS

Construction of plasmids

The dCas13X.1 and mini-dCas13X.1 proteins were human codon optimized and flanked with NLS^{SV40} (PKKKRKV) or bpNLS^{SV40} (KRTADGSEFESPKKKRKV) and then fused to the ADARdd protein, the deaminase in the RESCUE-S editor, via a glycine-serine linker to constitute the different base editors. They were expressed by broad-spectrum promoters (cytomegalovirus promoter was used in HEK293T cells *in vitro*, and chicken b-actin hybrid promoter was used in viruses *in vivo*). *In vitro*, BFP fluorescence was also coexpressed with the editing system to indicate success transfection and expression of the vector in host cells. Different spacers were synthesized as oligos for cloning downstream of the human U6 promoter for expression with different sgRNA configurations in cells.

For the exploration of DR processing capability, the base editor and a reporter with an EGFP transcript harboring a DR sequence between its ATG and CDS sequence were cotransfected. Only when the protein loses DR processing function can GFP fluorescence be detected (Figure S1A).

For the fluorescent reporter system, the base editor and a mCherry reporter system containing an early stop codon TAG mutated from TGG codon (W) at its W148 encoding position were cotransfected (Figure 1A).

When exploring *Myo6*^{C442Y} or *OTOF*^{Q829X} *in vitro*, reporter vectors were constructed using mCherry and partial transcripts carrying corresponding mutations, as reported in the previous article.[16] mCherry fluorescence indicated success transfection in host cells (Figures 1E and S1).

All of the primers for PCR and gRNA sequences used in this study are provided in Tables S1 and S2.

Cell culture, transfection, and flow cytometry analysis

The mammalian cell line used in the study was HEK293T, which was cultured in the same way as in the previous article.[31]

For fluorescence detection, HEK293T was passaged at a ratio of 1:3 to 24-well plates. After 16 h, base editor and fluorescent reporter plasmid were cotransfected with polyethyleneimine (PEI) in a molar ratio of 1:1 in a total amount of 0.8 μg using the standard protocol.

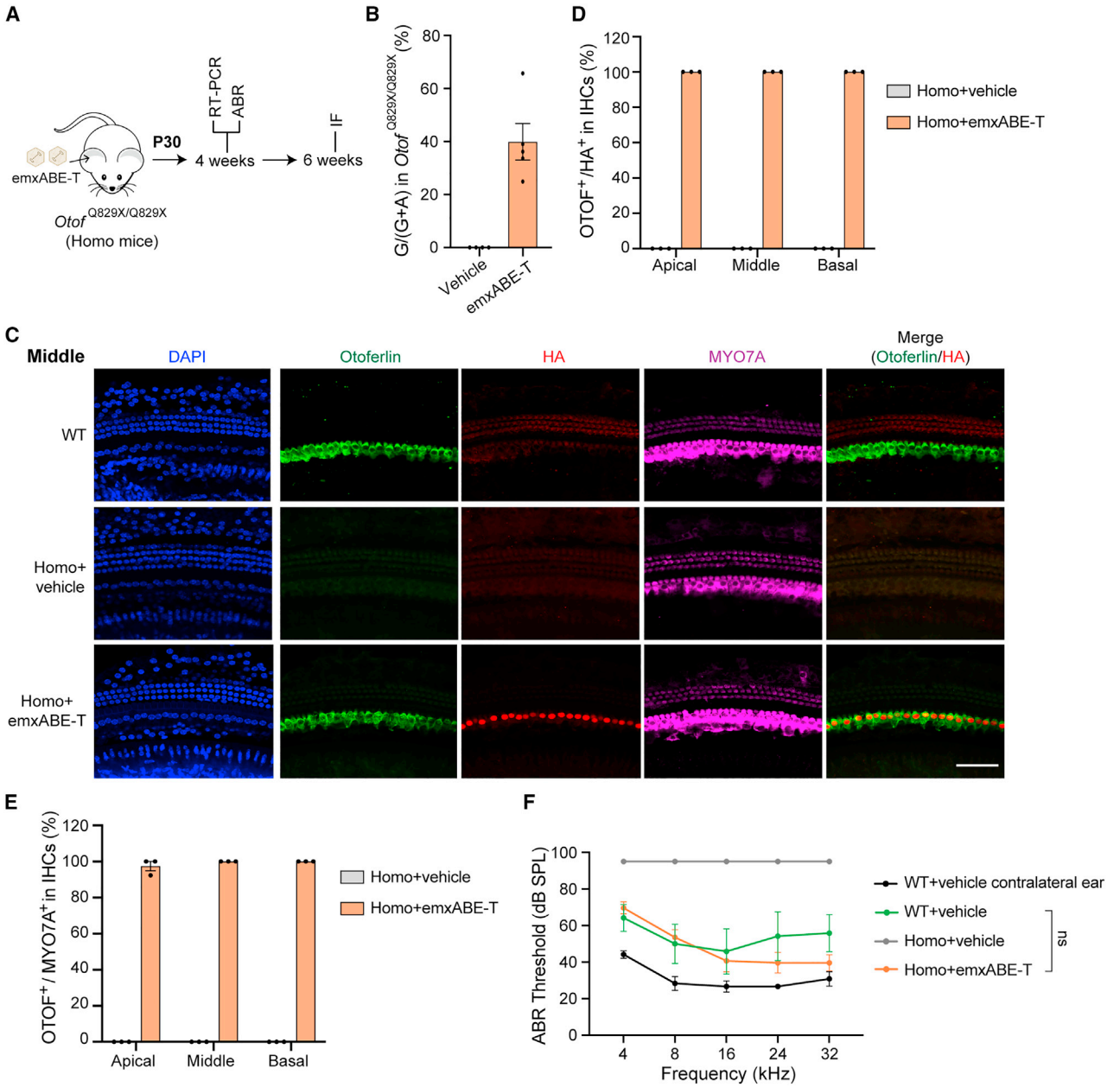

Figure 4. *In vivo* therapy of *Otof* ^{Q829X} mice with emxABE-T delivery at P30 by RW injection

(A) Diagrammatic workflow of the *in vivo* studies with emxABE-T delivered at P30 by AAV-HGHC in *Otof* $^{Q829X/Q829X}$ mice (hereafter marked Homo). (B) Deep-sequencing results after injection 4 weeks in the cochlea of *Otof* $^{Q829X/Q829X}$ mice at P30 (vehicle, n = 4; emxABE-T, n = 5). (C) Confocal of IHCs immunolabeled for otoferlin, IHC (MYO7A) and AAV-emxABE-T (HA) of middle cochlear turns after dosing 6 weeks. Scale bars: 50 μm. (D) The proportion of successful recovery of OTOF protein expression in IHC cells infected with the virus (HA$^+$). n = 3. (E) The OTOF recovery efficiency in all IHCs (MYO7A$^+$) are calculated by OTOF$^+$/MYO7A$^+$. n = 3. (F) ABR thresholds of mice for tone-burst stimuli are recorded 4 weeks after therapeutic injection (WT + vehicle contralateral ear, the contralateral ear from WT + vehicle group, n = 6; WT + vehicle, n = 6; Homo+vehicle, n = 5; Homo+emxABE-T, n = 14). Data are presented as mean ± SEM. Statistical tests were 2-way ANOVA with Bonferroni correction for multiple comparisons. See Table S6 for detailed data.

Cells were analyzed by Beckman cytoFLEX at 48 h after the transfection. Flow cytometry results were analyzed with FlowJo X (version 10.0.7).

For the exploration of *FANCC*, *SMAD4*, *Myo6*^{C442Y}, or *OTOF*^{Q829X} sites, HEK293T was passaged at a ratio of 1:3 to 6-well plates. After 16 h, plasmids were transfected with PEI in a molar ratio of 1:1 in a

total amount of 2 μg using the standard protocol. Cells were sorted by BD FACSAria III 48 h after the transfection.

RT-PCR and sequencing analysis

To analyze *in vitro* A-to-I base-editing efficiency, successfully transfected cells were sorted for RNA extraction at 48 h after transfection. For *in vivo* editing analysis, temporal bones were harvested at post-dosing 3 or 4 weeks from emxABE-T or untreated mice. Briefly, temporal bones were harvested, and the osseous spiral-shaped snail shells were removed carefully with microsurgical forceps under a dissection microscope. All of the soft tissues within the snail shell were collected, including cochlear modiolus and transferred to TRIzol (Invitrogen). Then, total RNA of sorted cells or soft tissues was isolated with RNA-easy isolation reagent according to the manufacturer's protocol and converted to cDNA using the reverse transcription kit (HiScript Q RT SuperMix for qPCR, Vazyme, Biotech, P611-01). The CRISPR RNA (crRNA) target sites were amplified from cDNAs with Phanta Max Super-Fidelity DNA Polymerase (Vazyme, P505-d1) for Sanger or deep sequencing methods.

Sanger sequencing results were analyzed with EditR 1.0.10 (https://moriaritylab.shinyapps.io/editr_v10/)[32] to quantify A-to-I conversion efficiency.

Targeted amplicon sequencing reads were demultiplexed using fastq-multx and trimmed using trim_galore (powered by Cutadapt 0.6.6). The cleaned pairs were then merged using FLASH version 1.2.11 and further analyzed using CRISPResso2[33] to identify the genome editing.

Analysis of RNA-seq results in HEK293T

RNA-seq reads were trimmed, and edit sites were identified as described previously.[15,16] SNPs filtering was done using the database downloaded from NCBI, 1000 Genomes Project (https://www.internationalgenome.org/) and the University of Washington Exome Sequencing Project (https://evs.gs.washington.edu/EVS/). We further annotated the SNVs using annotate_variation.pl in variant annotation tool ANNOVAR with gene-based annotation mode (-geneAnno) and the hg38 database (updated on January 5, 2023). The genes with nonsynonymous SNVs were collected for functional analysis using functional classification offered by the AmiGO webtool (based on the PANTHER database version 16.0), in which cellular processes from biological processes were focused for functional distribution analysis.

Venn plots were done by suma2Venn from R package maSigPro.

Analysis of RNA-seq results in mice

Transcriptome-wide sequencing was treated as described previously.[34] In brief, raw were cleaned using trim_galore and transcripts quantification was done by Salmon (version 1.5). The differential analysis between groups was conducted using a count-based method limma, and significantly expressed genes were screened by theBenjamini-Hochberg-adjusted p value (<0.05) and the fold change (>2).

Generation of *Otof* ^{Q829X} mouse model

Otof ^{Q829X} mice were generated in the C57BL/6J background using the CRISPR-Cas9 system. Mouse Otof exon 21 was deleted by CRISPR-Cas9 guided by 4 sgRNAs flanking exon 21 and replaced with the corresponding human exon carried Q829X mutation (Figure S4A). A total of 100 ng/μL spCas9 mRNA, 100 ng/μL sgRNA, and 100 ng/μL donor were mixed and then injected into the fertilized eggs to generate the F0 *Otof* ^{Q829X} mice. The mice were housed in an specific pathogen-free animal house (constant temperature of 22°C–25°C, relative humidity of 40%–70%) maintained on a 12-h light/dark cycle and provided food and water *ad libitum*. All of the experimental protocols were approved by the Animal Care and Use Committee of the Institute of Neuroscience, Chinese Academy of Sciences, Shanghai, China, and HuidaGene Therapeutics Co., Ltd., China. Because C57BL/6J mice have age-related hearing loss due to the homozygous *Cdh23*^{ahl} allele, the *Otof* ^{Q829X} mice were crossed with FVB/NCrl mice, and offspring without *Cdh23*^{ahl} were selected. These mice were used as parental stock and were mated and passaged. These mice produce offspring that do not have the *Cdh23*^{ahl} allele and can be used directly in therapeutic studies.

AAV virus production

The emxABE-T plasmid was sequenced before packaging into the AAV-HGHC vector, and the AAV vectors were packaged by HuidaGene Therapeutics Co., Ltd. and purified by iodixanol density gradient centrifugation. The vector titer was determined by qPCR specific for the inverted terminal repeat of the virus.

Inner ear injections

The inner ear injection method used in this study was the same as previously described.[16,35] For P0−P3 and P5−P7 mice injection, *Otof* $^{Q829X/Q829X}$ mouse pups were anesthetized by immersion in ice water. Upon anesthesia, a postauricular incision was made to expose the otic bulla and the stapedial artery. A total of 500 nL of AAV-HGHC-emxABE-T virus per cochlea was injected into the SM through the soft cochlear lateral wall at P0−P3. A total of 1,000 nL of AAV-HGHC-emxABE-T virus per cochlea was injected through the RW at P5−P7. P30 mice were anesthetized with an intraperitoneal injection of xylazine (10 mg/kg) and ketamine (100 mg/kg); then, 1,000–1,500 nL of AAV-HGHC-emxABE-T virus per cochlea was injected through the RW using glass micropipettes on the Nanoliter Microinjection System (World Precision Instruments, Sarasota, FL) at a rate of 169 nL/min at P30 mice. The location of the basal cochlear turn is distinguished by its anatomy in relation to the stapedius artery. For RW injection, a hole was made in the otic bulla and widened to visualize the stapedial artery and the RW membrane. After the injection, a suture was used to close the incision, and the RW membrane niche was quickly sealed with a small plug of adipose tissue to avoid leakage. Then, the bony defects of the otic bulla were sealed using tissue adhesive. The mice were placed on a 42°C heating pad for recovery. The pups were returned to their mother after they were fully recovered. Standard postoperative care was applied after the surgery. A dose of 1.25×10^{10} vg/ear was defined as a low dose, greater than 1.25×10^{10} vg/ear but not greater than 5×10^{10} vg/ear

was defined as a medium dose, and 9.21×10^{10} vg/ear was defined as a high dose.

Hearing tests

ABR and DPOAE measurements were performed in the same manner as described earlier using an RZ6 Acoustic System (Tucker-Davis Technologies, Alachua, FL).[16,35] The mice were placed into a sound-proof chamber. ABRs and DPOAEs were recorded during the same session. Mice of either sex were anesthetized with intraperitoneal injections of xylazine (10 mg/kg) and ketamine (100 mg/kg). For closed-field ABR, a subcutaneous needle electrode was inserted into the subcutaneous tissues of the vertex (reference electrode), mastoid (recording electrode), and rump (ground electrode) of the animals. ABR potentials were evoked and subsequently amplified 10,000 times with 1,024 responses and band-pass filtered at 300 Hz–3 kHz at each sound pressure level (SPL). Tone-burst sound stimuli were presented at 4, 8, 16, 24, and 32 kHz to test the frequency-specific hearing thresholds. The threshold of a certain frequency was determined as the lowest SPL at which any ABR wave could be detected upon visual inspection and could be repeated. The wave I amplitude of the ABR was measured from the peak of wave I to the following trough. The mice were placed on a heating pad covered by a sterile drape to maintain their body temperature during auditory ABR and DPOAE tests. Data were analyzed and plotted using GraphPad Prism 8, and threshold averages ± SEMs are presented unless otherwise stated.

Confocal microscopy and cell counting

Cochlear whole mounts of emxABE-T or noninjected ears were immunostained, as previously described.[13] The temporal bones of mice were harvested, cleaned, and placed in 4% formaldehyde for 2 h at room temperature or overnight at 4°C followed by decalcification for 36–72 h with 10% EDTA (pH 7.4) at 4°C. The sensory epithelium was then dissected and stored in PBS at 4°C until staining. Tissues were permeabilized with 0.1% Triton X-100 for 1 h, blocked with 10% normal donkey serum, and then incubated with anti-MYO7A primary antibody (1:500 dilution, Proteus BioSciences) for labeling hair cells, CTBP2 (1:200 dilution, BD Bioscience) for labeling synaptic ribbons, hemagglutinin (HA) (1:50 dilution, Roche) for labeling HA tag, and OTOF (1:100 dilution, Abcam) for labeling otoferlin protein overnight at 4°C. Then, the samples were rinsed 3 times in PBS and incubated with the following secondary antibodies for 2 h at room temperature: Alexa Fluor 488 AffiniPure Donkey Anti-Rabbit immunoglobulin G (IgG) (heavy and light chains [H + L]) (1:800, 711-545-152, Jackson ImmunoResearch Laboratories), Alexa Fluor 488 AffiniPure Donkey Anti-Mouse IgG (H + L) (1:1,000, 715-545-151, Jackson ImmunoResearch Laboratories), Cy5 AffiniPure Donkey Anti-Rat IgG (H + L) (1:1,000, 712-175-153, Jackson ImmunoResearch Laboratories), Cy3 AffiniPure Donkey Anti-Rabbit IgG (H + L) (1:1,000, 711-165-152, Jackson ImmunoResearch Laboratories) were used for detection. DAPI was used to label the nuclei (1:800 dilution, Sigma Aldrich). After antibody incubation, slides were washed and covered with mountant (Life Technologies). Images were acquired on a Nikon C2+ scanning confocal microscope with air objective for low-magnification images and oil-immersion objective for high-magnification images to collect all of the fluorescent z stack images. Images were edited by the ImageJ plugin. The tools in the ImageJ software were used for counting the number of OTOF/HA/Myosin7a$^+$ hair cells per 100-mm length along the sensory epithelia in the apical, middle, and basal turns of the cochlea. Synaptic ribbon (immunolabeled with CtBP2) numbers were also manually counted using ImageJ under same criteria for analysis of the different samples. Adobe Illustrator CS6 was used for organizing figures.

Statistical analysis

Statistical analyses were performed with GraphPad Prism version 8.0. Two groups were compared using unpaired two-tailed Student's t tests. To compare more than two groups of ABRs, two-way ANOVA with Bonferroni correction for multiple comparisons was used. Differences in means were considered statistically significant at $p < 0.05$. The significance levels were $^*p < 0.05$, $^{**}p < 0.01$, $^{***}p < 0.001$, and $^{****}p < 0.0001$. The mice were randomly assigned to different test groups. Data are presented as the mean ± SEM.

DATA AND MATERIALS AVAILABILITY

All data and materials associated with this study are presented in the paper or in the supplemental information. Raw sequencing files have been uploaded to NCBI's Sequence Read Archive. Accession number: PRJNA977802 for results from HEK293T and PRJNA977596 for results from mice.

SUPPLEMENTAL INFORMATION

Supplemental information can be found online at https://doi.org/10.1016/j.ymthe.2023.10.019.

ACKNOWLEDGMENTS

We thank Alvin Luk for helpful discussions and comments on this manuscript. This work was supported by HuidaGene Therapeutics Co., Ltd., the National Natural Science Foundation of China (nos. 81970872 and 82122019), the Shanghai Municipal Science and Technology Major Project (no. 21JC1404000), and the Shanghai Key Laboratory of Translational Medicine on Ear and Nose Diseases (14DZ2260300).

AUTHOR CONTRIBUTIONS

Yuanyuan Xue, Y.T., and Xing Wang designed and conducted the experiments. Yuanyuan Xue, S.C., B.Y., L.B., H.J., Xueling Wang, W.K., and Z.C. performed mouse experiments. Xing Wang, Y.L., L.C., and Yanwe Xie performed the sequencing data analysis. J.L., Q.X., and L.S. provided key advice for this project. H.Y., L.S., Xuan Yao, H.W., and Y.S. supervised the whole project. H.Y., Yuanyuan Xue, and Xing Wang. wrote the manuscript, and all of authors contributed to the editing of the manuscript. Y.S. played an important role in article revision.

DECLARATION OF INTERESTS

Xing Wang disclosed a patent application related to this work. L.S. and Y.X. disclosed a patent application related to the AAV vector used in this work. H.Y. is the cofounder of HuidaGene Therapeutics Co., Ltd. The remaining authors declare no competing interests.

REFERENCES

1. Morton, C.C., and Nance, W.E. (2006). Newborn hearing screening–a silent revolution. N. Engl. J. Med. *354*, 2151–2164. https://doi.org/10.1056/NEJMra050700.
2. GBD 2019 Hearing Loss Collaborators (2021). Hearing loss prevalence and years lived with disability, 1990-2019: findings from the Global Burden of Disease Study 2019. Lancet *397*, 996–1009. https://doi.org/10.1016/S0140-6736(21)00516-X.
3. Omichi, R., Shibata, S.B., Morton, C.C., and Smith, R.J.H. (2019). Gene therapy for hearing loss. Hum. Mol. Genet. *28*, R65–R79. https://doi.org/10.1093/hmg/ddz129.
4. Thorpe, R.K., Azaiez, H., Wu, P., Wang, Q., Xu, L., Dai, P., Yang, T., Schaefer, G.B., Peters, B.R., Chan, K.H., et al. (2022). The natural history of OTOF-related auditory neuropathy spectrum disorders: a multicenter study. Hum. Genet. *141*, 853–863. https://doi.org/10.1007/s00439-021-02340-w.
5. Yasunaga, S., Grati, M., Cohen-Salmon, M., El-Amraoui, A., Mustapha, M., Salem, N., El-Zir, E., Loiselet, J., and Petit, C. (1999). A mutation in OTOF, encoding otoferlin, a FER-1-like protein, causes DFNB9, a nonsyndromic form of deafness. Nat. Genet. *21*, 363–369. https://doi.org/10.1038/7693.
6. Pangrsic, T., Lasarow, L., Reuter, K., Takago, H., Schwander, M., Riedel, D., Frank, T., Tarantino, L.M., Bailey, J.S., Strenzke, N., et al. (2010). Hearing requires otoferlin-dependent efficient replenishment of synaptic vesicles in hair cells. Nat. Neurosci. *13*, 869–876. https://doi.org/10.1038/nn.2578.
7. Migliosi, V., Modamio-Høybjør, S., Moreno-Pelayo, M.A., Rodríguez-Ballesteros, M., Villamar, M., Tellería, D., Menéndez, I., Moreno, F., and Del Castillo, I. (2002). Q829X, a novel mutation in the gene encoding otoferlin (OTOF), is frequently found in Spanish patients with prelingual non-syndromic hearing loss. J. Med. Genet. *39*, 502–506. https://doi.org/10.1136/jmg.39.7.502.
8. Wilson, B.S., and Dorman, M.F. (2008). Cochlear implants: current designs and future possibilities. J. Rehabil. Res. Dev. *45*, 695–730. https://doi.org/10.1682/jrrd.2007.10.0173.
9. McDermott, H.J. (2004). Music perception with cochlear implants: a review. Trends Amplif. *8*, 49–82. https://doi.org/10.1177/108471380400800203.
10. Reiss, L.A.J., Kirk, J., Claussen, A.D., and Fallon, J.B. (2022). Animal Models of Hearing Loss after Cochlear Implantation and Electrical Stimulation. Hear. Res. *426*, 108624. https://doi.org/10.1016/j.heares.2022.108624.
11. Karimnejad, K., Akhter, A.S., Walen, S.G., and Mikulec, A.A. (2017). The temporoparietal fascia flap for coverage of cochlear reimplantation following extrusion. Int. J. Pediatr. Otorhinolaryngol. *94*, 64–67. https://doi.org/10.1016/j.ijporl.2017.01.020.
12. Akil, O., Dyka, F., Calvet, C., Emptoz, A., Lahlou, G., Nouaille, S., Boutet de Monvel, J., Hardelin, J.P., Hauswirth, W.W., Avan, P., et al. (2019). Dual AAV-mediated gene therapy restores hearing in a DFNB9 mouse model. Proc. Natl. Acad. Sci. USA. *116*, 4496–4501. https://doi.org/10.1073/pnas.1817537116.
13. Al-Moyed, H., Cepeda, A.P., Jung, S., Moser, T., Kügler, S., and Reisinger, E. (2019). A dual-AAV approach restores fast exocytosis and partially rescues auditory function in deaf otoferlin knock-out mice. EMBO Mol. Med. *11*, e9396. https://doi.org/10.15252/emmm.201809396.
14. Tang, H., Wang, H., Wang, S., Hu, S.W., Lv, J., Xun, M., Gao, K., Wang, F., Chen, Y., Wang, D., et al. (2023). Hearing of Otof-deficient mice restored by trans-splicing of N- and C-terminal otoferlin. Hum. Genet. *142*, 289–304. https://doi.org/10.1007/s00439-022-02504-2.
15. Xu, C., Zhou, Y., Xiao, Q., He, B., Geng, G., Wang, Z., Cao, B., Dong, X., Bai, W., Wang, Y., et al. (2021). Programmable RNA editing with compact CRISPR-Cas13 systems from uncultivated microbes. Nat. Methods *18*, 499–506. https://doi.org/10.1038/s41592-021-01124-4.
16. Xiao, Q., Xu, Z., Xue, Y., Xu, C., Han, L., Liu, Y., Wang, F., Zhang, R., Han, S., Wang, X., et al. (2022). Rescue of autosomal dominant hearing loss by in vivo delivery of mini dCas13X-derived RNA base editor. Sci. Transl. Med. *14*, eabn0449. https://doi.org/10.1126/scitranslmed.abn0449.
17. Katrekar, D., Chen, G., Meluzzi, D., Ganesh, A., Worlikar, A., Shih, Y.R., Varghese, S., and Mali, P. (2019). In vivo RNA editing of point mutations via RNA-guided adenosine deaminases. Nat. Methods *16*, 239–242. https://doi.org/10.1038/s41592-019-0323-0.
18. Abudayyeh, O.O., Gootenberg, J.S., Franklin, B., Koob, J., Kellner, M.J., Ladha, A., Joung, J., Kirchgatterer, P., Cox, D.B.T., and Zhang, F. (2019). A cytosine deaminase for programmable single-base RNA editing. Science *365*, 382–386. https://doi.org/10.1126/science.aax7063.
19. Chen, P.J., Hussmann, J.A., Yan, J., Knipping, F., Ravisankar, P., Chen, P.F., Chen, C., Nelson, J.W., Newby, G.A., Sahin, M., et al. (2021). Enhanced prime editing systems by manipulating cellular determinants of editing outcomes. Cell *184*, 5635–5652.e29. https://doi.org/10.1016/j.cell.2021.09.018.
20. Roux, I., Safieddine, S., Nouvian, R., Grati, M., Simmler, M.C., Bahloul, A., Perfettini, I., Le Gall, M., Rostaing, P., Hamard, G., et al. (2006). Otoferlin, defective in a human deafness form, is essential for exocytosis at the auditory ribbon synapse. Cell *127*, 277–289. https://doi.org/10.1016/j.cell.2006.08.040.
21. Pelliccia, P., Venail, F., Bonafé, A., Makeieff, M., Iannetti, G., Bartolomeo, M., and Mondain, M. (2014). Cochlea size variability and implications in clinical practice. Acta Otorhinolaryngol. Ital. *34*, 42–49.
22. Song, L., McGee, J., and Walsh, E.J. (2006). Frequency- and level-dependent changes in auditory brainstem responses (ABRS) in developing mice. J. Acoust. Soc. Am. *119*, 2242–2257. https://doi.org/10.1121/1.2180533.
23. Akil, O., Seal, R.P., Burke, K., Wang, C., Alemi, A., During, M., Edwards, R.H., and Lustig, L.R. (2012). Restoration of hearing in the VGLUT3 knockout mouse using virally mediated gene therapy. Neuron *75*, 283–293. https://doi.org/10.1016/j.neuron.2012.05.019.
24. Dulon, D., Papal, S., Patni, P., Cortese, M., Vincent, P.F., Tertrais, M., Emptoz, A., Tlili, A., Bouleau, Y., Michel, V., et al. (2018). Clarin-1 gene transfer rescues auditory synaptopathy in model of Usher syndrome. J. Clin. Invest. *128*, 3382–3401. https://doi.org/10.1172/JCI94351.
25. Isgrig, K., Shteamer, J.W., Belyantseva, I.A., Drummond, M.C., Fitzgerald, T.S., Vijayakumar, S., Jones, S.M., Griffith, A.J., Friedman, T.B., Cunningham, L.L., and Chien, W.W. (2017). Gene Therapy Restores Balance and Auditory Functions in a Mouse Model of Usher Syndrome. Mol. Ther. *25*, 780–791. https://doi.org/10.1016/j.ymthe.2017.01.007.
26. Pan, B., Askew, C., Galvin, A., Heman-Ackah, S., Asai, Y., Indzhykulian, A.A., Jodelka, F.M., Hastings, M.L., Lentz, J.J., Vandenberghe, L.H., et al. (2017). Gene therapy restores auditory and vestibular function in a mouse model of Usher syndrome type 1c. Nat. Biotechnol. *35*, 264–272. https://doi.org/10.1038/nbt.3801.
27. Taiber, S., Cohen, R., Yizhar-Barnea, O., Sprinzak, D., Holt, J.R., and Avraham, K.B. (2021). Neonatal AAV gene therapy rescues hearing in a mouse model of SYNE4 deafness. EMBO Mol. Med. *13*, e13259. https://doi.org/10.15252/emmm.202013259.
28. Minoda, R., Miwa, T., Ise, M., and Takeda, H. (2015). Potential treatments for genetic hearing loss in humans: current conundrums. Gene Ther. *22*, 603–609. https://doi.org/10.1038/gt.2015.27.
29. Kim, D., Luk, K., Wolfe, S.A., and Kim, J.S. (2019). Evaluating and Enhancing Target Specificity of Gene-Editing Nucleases and Deaminases. Annu. Rev. Biochem. *88*, 191–220. https://doi.org/10.1146/annurev-biochem-013118-111730.
30. Katrekar, D., Yen, J., Xiang, Y., Saha, A., Meluzzi, D., Savva, Y., and Mali, P. (2022). Efficient in vitro and in vivo RNA editing via recruitment of endogenous ADARs using circular guide RNAs. Nat. Biotechnol. *40*, 938–945. https://doi.org/10.1038/s41587-021-01171-4.
31. Wang, X., Zhang, R., Yang, D., Li, G., Fan, Z., Du, H., Wang, Z., Liu, Y., Lin, J., Wu, X., et al. (2023). Develop a Compact RNA Base Editor by Fusing ADAR with Engineered EcCas6e. Adv. Sci. *10*, e2206813. https://doi.org/10.1002/advs.202206813.
32. Kluesner, M.G., Nedveck, D.A., Lahr, W.S., Garbe, J.R., Abrahante, J.E., Webber, B.R., and Moriarity, B.S. (2018). EditR: A Method to Quantify Base Editing from Sanger Sequencing. CRISPR J. *1*, 239–250. https://doi.org/10.1089/crispr.2018.0014.
33. Clement, K., Rees, H., Canver, M.C., Gehrke, J.M., Farouni, R., Hsu, J.Y., Cole, M.A., Liu, D.R., Joung, J.K., Bauer, D.E., and Pinello, L. (2019). CRISPResso2 provides accurate and rapid genome editing sequence analysis. Nat. Biotechnol. *37*, 224–226. https://doi.org/10.1038/s41587-019-0032-3.
34. Li, J., Shen, Z., Liu, Y., Yan, Z., Liu, Y., Lin, X., Tang, J., Lv, R., Geng, G., Xiong, Z.Q., et al. (2023). A high-fidelity RNA-targeting Cas13 restores paternal Ube3a expression and improves motor functions in Angelman syndrome mice. Mol. Ther. *31*, 2286–2295. https://doi.org/10.1016/j.ymthe.2023.02.015.
35. Zhao, Y., Zhang, L., Wang, D., Chen, B., and Shu, Y. (2022). Approaches and Vectors for Efficient Cochlear Gene Transfer in Adult Mouse Models. Biomolecules *13*, 38. https://doi.org/10.3390/biom13010038.